

Far-field sensitivity of droplet generation: Exponential scaling and cutoff

Zehao Pan and Hsueh-Chia Chang*

Department of Chemical and Biomolecular Engineering, University of Notre Dame, Notre Dame, Indiana 46556-5637, USA



(Received 14 January 2019; published 23 October 2019)

By smoothing the length-scale independent conic interface under an electric field into a pendant meniscus with finite curvature, dripping dynamics with a unique far-field sensitivity is observed. Two distinct dripping modes are detected: a microdripping regime whose droplet size is independent of the far field and a dripping regime whose droplet size depends on the far field exponentially. The exponential sensitivity is the result of a universal logarithm dependence of the Maxwell force on the droplet dimension for the pendant drop interface topology and the field independence of the former is due to the cutoff of this dependence by the orifice diameter. Universal self-similar scaling based on the local analysis of this dripping droplet is able to collapse the data over a large window of operating parameters. It hence allows precise tuning of the droplet size with this droplet generation mechanism.

DOI: [10.1103/PhysRevFluids.4.101701](https://doi.org/10.1103/PhysRevFluids.4.101701)

Droplet generation is a common phenomenon that is widely observed in daily life and has many microfluidic applications. At microscale, the dominant driving force is not gravity but rather shear stress [1–4], capillary pressure gradient [5–7], or cross-interface drag [8] forces. Electric field is also used to generate droplets [9], sometimes in conjunction with flow focusing [10] and sometimes through electrowetting [11,12] to suppress capillary and other instabilities. Droplet pinch-off by electric field often involves conic interfaces with universal self-similar scaling that is independent of far-field conditions [13]. The field and length-scale independent features, such as the 49° Taylor cone angle [14] with a DC (direct current) field, its 11° AC (alternating current) analog [15], and electrowetting dynamic contact angles, make it difficult to control the droplet size with an external field. As in the classical “lightning rod” phenomenon, conic or wedge geometries also produce high field and high viscous dissipation that lead to uncontrollable discharges and low droplet generation rates.

We have recently shown that AC electrospray in an immersed oil (iACE) generates droplets by a microdripping mechanism that is also insensitive to the far field [16]. (As is consistent with the flow-focusing literature, we use the terminology “dripping” when conic interfaces are absent, even though electric force is the dominant force.) The high-frequency AC field minimizes charge buildup and the high extensional viscosity of dispersed phase with a polymer additive suppresses cone formation and delays the pinching dynamics to minimize electrocoalescence. Instead, a pendant-shape droplet appears at the orifice, as if being pulled by gravity even if gravitational effects are absent, and introduces a local length scale, the orifice diameter d_{tip} , that disrupts the local similarity and controls the droplet size. Using a much less viscous oil phase in this work, we have identified a dripping regime where the droplet size has a strong exponential dependence on the applied electric field which is in contrast to the power-law dependence in actively controlled microfluidic devices [17].

*Author to whom correspondence should be addressed: hchang@nd.edu

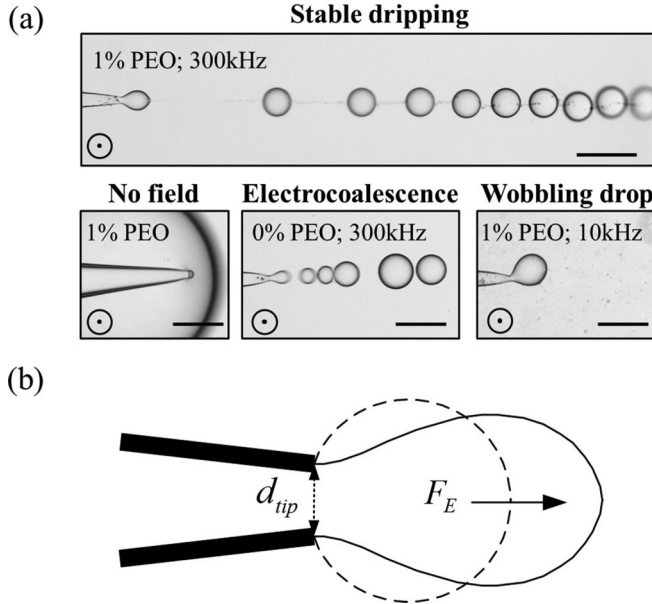


FIG. 1. (a) Snapshots of stable iACE dripping, buoyancy controlled growth without an electric field, iACE with electrocoalescence, and wobbling with different PEO concentration (w/w) in the dispersed phase and alternating frequency. The direction of gravity points out of the page as indicated by the arrows. Scale bar is 200 μm . (b) Stretching of a spherical drop at the end of a nozzle into a pendant droplet by an axial Maxwell force.

This leads to a dramatic threefold increase in the droplet size with just 10% change in the voltage. We carry out an in-depth analysis of the iACE dripping mechanism of these pendant-shape droplets and show that the unique far-field sensitivity is due to a shape-sensitive singular electric field at a growing droplet that is distinct from conic and other interface topology. The resulting scaling theory allows us to obtain monodispersed microemulsion whose droplet size can be tuned with a simple adjustment of the electric potential or applied pressure.

We used the experimental setup described earlier [16]. The dispersed phase consists of 1% (w/w) PEO (polyethylene oxide, 400 000 MW) and 100 mM potassium chloride (KCl) dissolved in deionized water. The continuous phase was HFE7500 containing 2% (w/w) perfluoropolyether (PFPE) and polyethylene glycol (PEG) block copolymer surfactant (RAN Biotechnologies, Beverly, MA) to reduce the surface tension γ to 7.8 mN/m and stabilize the emulsion after generation. The spacing L between the capillary tip and the planar indium tin oxide glass electrode was 4.0 mm. In the experiments shown below, three different tip diameters of the micropipettes were used. The droplet diameter was measured by analyzing 30 random droplets imaged by a CCD camera through an inverted microscope.

We had utilized a whipping instability induced by the PEO additive in a viscous mineral oil to prevent electrocoalescence by charging the drops and the connecting filaments with conductive polarization [16]. The helical spiraling motion of the whipping filament displaces two adjacent droplets in the transverse direction to eliminate the dipolar attraction. The whipping instability, however, also introduces a wobbling motion at the tip during droplet formation that can corrupt monodispersity in a low viscosity environment [see last frame of Fig. 1(a)].

With the less viscous continuous fluorinated oil used in the current study and with PEO addition to increase the extension viscosity of the dispersed phase, the ejected droplets are sufficiently separated from the nascent droplet in the high-field region near the tip. Consequently, droplet coalescence by dipolar attraction is avoided and an AC frequency higher than the inverse RC time

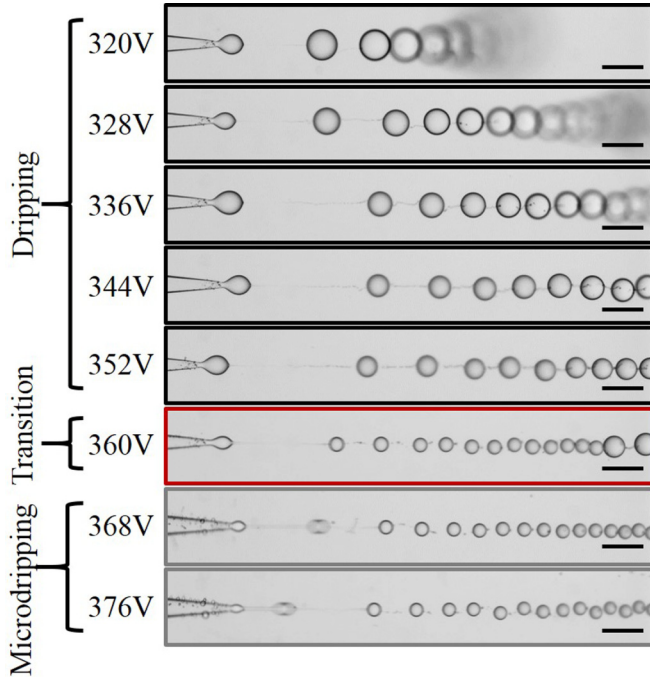


FIG. 2. Immersed AC electrospray droplet generation at different applied potential. $P_{app} = 4.1$ kPa; $d_{tip} = 24 \mu\text{m}$. Droplets defocused downstream due to the buoyancy effect. Scale bar is $200 \mu\text{m}$.

can be used to eliminate conductive polarization responsible for both the whipping instability and droplet wobbling at the tip. The RC time is the product of the electrolyte resistance across the tip and the Debye layer capacitance [18] and its inverse is about 10 kHz for the aqueous solution containing 100 mM KCl sprayed from a typical tip diameter of $10 \mu\text{m}$. When the field frequency is at 10 kHz or below, the droplet at the tip wobbles and pinches off irregularly as shown in Fig. 1(a). The wobbling and the whipping instabilities disappear beyond 10 kHz and the droplet generation dynamics and droplet size distribution stabilize beyond 100 kHz.

Figure 1(b) illustrates the observed generic droplet dripping dynamics of iACE. After an initial stage of radially symmetric growth, the axial Maxwell force F_E due to the interfacial electric Maxwell stress at the tip, stretches the drop to form a neck. The “pendant” droplet continues to grow as it elongates until it pinches off at the neck. Thin filaments due to the viscoelastic properties of PEO [19] connect the generated droplets but they break up downstream without affecting the droplet size.

We first tested the droplet size dependence as a function of the applied potential (from 280 to 420 V) at a constant P_{app} of 4.1 kPa for d_{tip} of $24 \mu\text{m}$, as shown in Fig. 2. When U_{app} was lower than 320 V, the meniscus grew out of the tip due to the applied pressure until it was pinched off by buoyancy force. The resulting droplet diameter d_{drop} is hence determined by $\pi d_{tip}\gamma = \Delta\rho g(\pi d_{drop}^3/6)$, where $\Delta\rho = 0.614 \text{ g/cm}^3$ is the density difference between the water and the oil phase. The expression yields $d_{drop} = 570 \mu\text{m}$ which agrees roughly with the measured value of $\sim 700 \mu\text{m}$.

Buoyancy becomes unimportant beyond a critical U_{app} of about 320 V, when the droplets are ejected before they reach the size estimated above to generate monodispersed suspensions with d_{drop} smaller than $180 \mu\text{m}$. Electric force now dominates over buoyancy force, and three distinct regimes—dripping, transition, and microdripping—can be identified based on the different behaviors of the droplet size as a function of U_{app} (see Fig. 2). In the dripping regime from 320 to

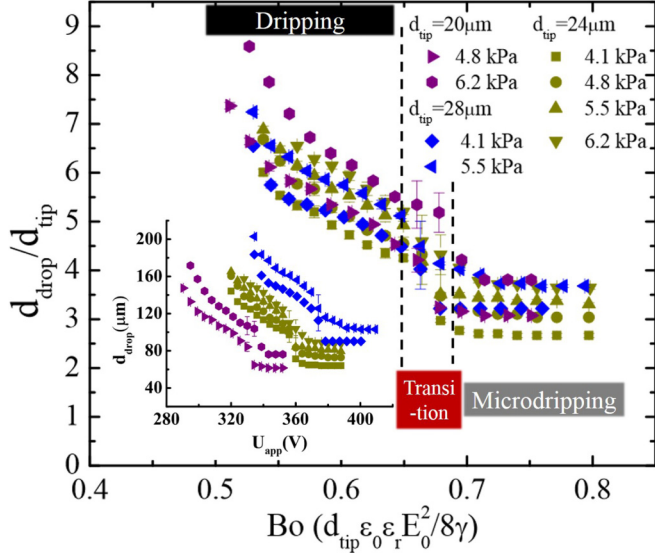


FIG. 3. Collapse of data on droplet diameter as a function of the electrical Bond number Bo . Inset: droplet diameter as a function of U_{app} at different values of P_{app} and d_{tip} .

352 V, the droplet size decreases precipitously as U_{app} increases. A 10% increase in the applied voltage reduces the droplet size by three folds. Because of this high sensitivity, only a small window of voltage gives rise to droplets that are larger than the tip diameter and are unaffected by buoyancy effects. The dripping phenomenon is, however, very robust in this window. The droplets are monodispersed in the dripping regime, with a coefficient of variation (CV) below 3.0%. In the transition regime between dripping and microdripping, a bimodal size distribution is observed, where the system switches back and forth between the dripping regime and the microdripping regime with two distinct droplet sizes with a timescale of about 100 ms. In the microdripping regime from 368 to 376 V, the droplets recover monodispersity, but the droplet size saturates to a value independent of U_{app} up to a value of 384 V where charge-induced jetting and whipping instability begins to affect the monodispersity. This is the field-insensitive microdripping regime.

At higher applied pressures, the same three regimes can be identified with the same transition voltages but the droplet size is shifted upwards (see inset of Fig. 3). This suggests that the pinching time is significantly long such that the flow into the pinching droplet controls the final size of the ejected droplets. Experiments with two other tip diameters were also performed (inset of Fig. 3). Even though the three regimes are found in all cases, they occur at different ranges of U_{app} and there is a clear shift to higher transition voltages with larger d_{tip} . This suggests the different regimes are associated with the radius of curvature of the nascent droplet with diameter d_{tip} . We hence expect the transition between the two dripping regimes is defined by a critical static condition related to the voltage and tip diameter but the actual droplet size involves viscous flow and is hence also dependent on the applied pressure.

Inertial effects on both velocity and pressure are ruled out with a Reynolds number Re estimate of less than 0.5 and a Weber number We of less than 0.1, based on a measured fluid velocity of no more than 200 cm/s at the tip. Thus, inertial jetting cannot happen in iACE [2,20]. Hence, the only possible mechanism for droplet ejection is the classical dripping mechanism due to a balance between the Maxwell force F_E and the surface tension force that holds the finite-curvature drop to the capillary at the contact line. The applied pressure does not produce a net axial force, as its isotropic nature produces a radial expansion instead of an axial elongation and necking of the droplet necessary for dripping.

This static force balance defines an electrical bond number Bo representing the ratio of the Maxwell force $F_E = (\epsilon_0 \epsilon_r E_0^2 / 2) \pi d_{\text{tip}}^2 / 4$ to surface tension force, $\pi d_{\text{tip}} \gamma$, at the orifice contact line for a droplet with diameter d_{tip} :

$$\text{Bo} = \frac{d_{\text{tip}} \epsilon_0 \epsilon_r E_0^2}{8\gamma}, \quad (1)$$

where ϵ_0 is the vacuum permittivity, ϵ_r the relative permittivity of the fluorinated oil (5.8), and E_0 the electric field at the orifice. The dispersed droplet phase is a conducting electrolyte and is hence assumed to be at constant potential—the electric field responsible for the Maxwell force is entirely in the oil phase.

In contrast to the field on a conic meniscus, electric field E_0 on the pendant droplet is described by a far-field sensitive universal scaling in the limit of $d_{\text{tip}} \ll L$, where $L = 4.0$ mm is the separation between the tip of the micropipette and the counterelectrode. This universal field depends only on d_{tip} , L , and the applied potential U_{app} , with d_{tip} replaced by the droplet radius of curvature when the latter becomes larger than the orifice dimension. It is insensitive to other length scales or geometries away from the tip of the pendant droplet. This universal field was first derived by Eyring *et al.* by studying an electrode with a hyperboloid geometry [21],

$$E_0 = \frac{2\sqrt{2}U_{\text{app}}}{d_{\text{tip}} \ln\left(\frac{8L}{d_{\text{tip}}}\right)}. \quad (2)$$

The same scaling for E_0 was later derived for a semi-infinite conducting cylindrical rod with a spherical tip by Jones and Thong [22], also in the limit when the tip curvature is much smaller than the electrode separation. Their expression differs from that of Eyring *et al.* and other expressions for E_0 by a unit-order factor [21,23]. The derivation was done for a capillary that is oriented vertically towards a planar electrode. However, as the maximum field at the tip is oriented in the axial direction of the cylinder, the field line emanating from the tip of a horizontal electrode begins in the axial direction of the cylinder before arcing sharply towards the electrode (see Fig. 2 of Jones and Thong [22]). Hence, the arc length of this field line is close to the tip-plane separation and Jones and Thong were able to show that (2) applies for both horizontal and vertical cylinders. In addition, they show that it also works well for a finite length cylindrical electrode. It is hence a universal law for a pendant droplet electrode with a constant-curvature tip. We note the electric field emanating from an isolated spherical electrode, $U_{\text{app}}/d_{\text{tip}}$, is now modified by the factor $\ln(8L/d_{\text{tip}})$ because of the semi-infinite geometry due to the presence of the neck. Yet, the angle and radius of the neck do not appear to leading order. This logarithm scaling of the field is unique to the pendant droplet topology in the dripping regime and is the key to the exponential dependence of the droplet size on the far field.

We plot $d_{\text{drop}}/d_{\text{tip}}$ versus the dimensionless electric field Bo in Fig. 3. The proper scaling with respect to d_{tip} is evident by the collapse of the different transition regimes to a universal Bo between 0.65 and 0.68. This defines the critical electric field below which a droplet of diameter d_{tip} cannot be pulled off the capillary orifice.

As a droplet grows out of the orifice, the local curvature at the tip is no longer governed by d_{tip} but by d_{drop} instead. Replacing d_{tip} by d_{drop} in E_0 for the axial Maxwell force F_E on an arbitrary droplet, $(\epsilon_0 \epsilon_r E_0^2 / 2) \pi d_{\text{drop}}^2 / 4$, it is clear that the Maxwell force increases with the droplet size, with the scaling of inverse $\ln(8L/d_{\text{drop}})$, whereas the opposing surface tension force at the capillary contact line retains d_{tip} as its length scale and is independent of d_{drop} . Hence, below the critical electric field, the droplet must grow in size before it can be pulled off to undergo dripping. We estimate this droplet size d_E by first modifying E_0 to account for the a droplet radius that is larger than d_{tip} , $E_D = 2\sqrt{2}U_{\text{app}}/[d_E \ln(8L/d_E)]$.

Balancing this larger Maxwell force of the grown droplet to the capillary tension with length scale d_{tip} , we obtain the critical pinch-off droplet diameter d_E for electric fields lower than the

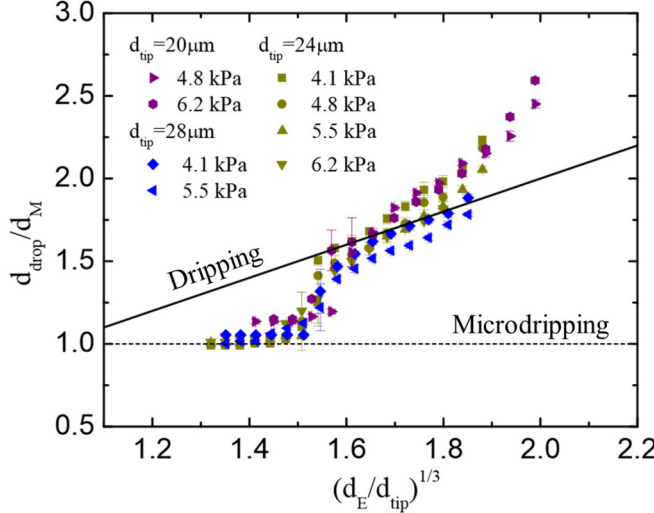


FIG. 4. Collapse of experimental data. Solid line: theoretical prediction for the dripping regime $d_{\text{drop}} = d_D$. Dashed line: theoretical prediction for the microdripping regime $d_{\text{drop}} = d_M$.

critical value $\text{Bo} = 0.65$.

$$d_E/8L = (d_{\text{tip}}/8L)^{-\sqrt{\text{Bo}}}. \quad (3)$$

This critical droplet size has an exponential dependence on Bo that originates from the logarithm scaling of (2). It is cut off beyond the critical electric field for d_{tip} , which is the lower bound for droplet diameters such that the sensitivity to the far field and L vanishes.

The above static analyses provide estimates for the critical droplet size for the droplet to be pulled off the capillary and undergo dripping by pinch-off. However, as the pinching time is significant, the droplet size after pinch-off is different from this value and is instead determined by pressure-driven flow through the orifice during pinch-off. For the microdripping regime, this duration is the Rayleigh capillary-viscous pinching time of $\tau = C^3 \eta^- d_{\text{tip}} / \gamma$, where C is a constant determined by the viscosity ratio η^-/η^+ (~ 15) [24] between the dispersed and the continuous phase, with the dispersed phase viscosity $\eta^- \sim 12 \text{ cp}$ [25]. The volume of the droplet then becomes $Q\tau$, where Q is the flow rate driven by P_{app} through the orifice [26]. Due to the converging conic geometry of the capillary, the hydrodynamic resistance is independent of the length of the capillary and is only a function of the tip diameter d_{tip} . This results in an expression of the droplet diameter in the microdripping regime that is independent of the far field and any length scale except d_{tip} [16]:

$$d_M = C(9 \tan \alpha / 64\gamma)^{1/3} (P_{\text{app}} - P_c)^{1/3} d_{\text{tip}}^{4/3}, \quad (4)$$

where α is the average half cone angle of the micropipette (5.7°). P_c is the threshold pressure for flow at the orifice that must be exceeded to counter achieve microdripping or dripping. It is experimentally measured to be around $8\gamma/d_{\text{tip}}$. The reason this value is roughly twice the capillary pressure at the tip could be attributed to the dynamic surface tension [27] at the growing interface. Based on the measured microdripping droplet size, C is fitted to be 5.3, a reasonable value when the inner phase viscosity exceeds the outer phase viscosity [24]. Experimental data for the average droplet diameter in the microdripping regime are collapsed based on this model, as shown in Fig. 4. Both the viscoelastic pinching time [28] and the pressure-driven growth time are calculated to be smaller than τ , thus as first-order approximation the predicted droplet generation frequencies of $1/\tau$ in the microdripping regime for $d_{\text{tip}} = 24 \mu\text{m}$ is 200 Hz, in good agreement with the measured value of 150 ± 10 Hz for all P_{app} acquired from the average of five consecutive frames of each experiment.

In the dripping regime, we change the droplet diameter from d_{tip} to d_E in the estimate for the viscous-capillary pinch-off time, $\tau_d = C^3 \eta^- d_E / \gamma$. This simple change in length scale produces an estimate for the droplet size in the dripping regime that is related to the size in the microdripping regime by a self-similar relationship:

$$\frac{d_{\text{drop}}}{d_M} = \left(\frac{d_E}{d_{\text{tip}}} \right)^{1/3}. \quad (5)$$

We are able to collapse the measured d_{drop} in both dripping regimes with this relationship and with the same value of $C = 5.3$ determined from the microdripping droplets. The scaling breaks down for very large droplets at low fields because the estimated capillary force based on a spherical drop with diameter d_{tip} is expected to be invalid for large droplets deformed by both electric and gravitational forces. The scaling collapse within a 100 V neighborhood of the transition voltage confirms the two mechanisms for droplet generation by an AC field. The critical static balance between electric and capillary forces defines the transition from dripping and microdripping at $d_{\text{drop}} = 3.5 d_{\text{tip}}$ of Fig. 3. The dripping mechanism requires the droplet to grow to a size larger than the tip diameter before the electric field can pinch it off and the higher field in the microdripping regime would eject the droplet as soon as it is formed at the tip. The theory also captures the droplet size determined by the applied pressure-driven flow from the conic orifice into the droplets on two sides of the transition voltage, with the microdripping drop size independent of the electric field contained in d_E since the drainage into the droplet during pinch-off begins at a field-independent droplet size of d_{tip} . The dripping regime, on the other hand, produces an exponential dependence of the droplet size on the electric field and hence can be used to dynamically tune droplet size without flow-driven shear force—a unique feature that is missing in other droplet generation mechanisms.

We acknowledge the support of a China Scholarship Council fellowship for Z.P. Z.P. and H.-C.C. are supported by NIH IMAT under Grant No. 1R21CA206904.

- [1] T. Thorsen, R. W. Roberts, F. H. Arnold, and S. R. Quake, Dynamic Pattern Formation in a Vesicle-Generating Microfluidic Device, *Phys. Rev. Lett.* **86**, 4163 (2001).
- [2] A. S. Utada, A. Fernandez-Nieves, H. A. Stone, and D. A. Weitz, Dripping to Jetting Transitions in Coflowing Liquid Streams, *Phys. Rev. Lett.* **99**, 094502 (2007).
- [3] A. J. deMello, Control and detection of chemical reactions in microfluidic systems, *Nature (London)* **442**, 394 (2006).
- [4] R. Dreyfus, P. Tabeling, and H. Willaime, Ordered and Disordered Patterns in Two-Phase Flows in Microchannels, *Phys. Rev. Lett.* **90**, 144505 (2003).
- [5] S. Sugiura, M. Nakajima, S. Iwamoto, and M. Seki, Interfacial tension driven monodispersed droplet formation from microfabricated channel array, *Langmuir* **17**, 5562 (2001).
- [6] R. Dangla, S. C. Kayi, and C. N. Baroud, Droplet microfluidics driven by gradients of confinement, *Proc. Natl. Acad. Sci. USA* **110**, 853 (2013).
- [7] C. Priest, S. Herminghaus, and R. Seemann, Generation of monodisperse gel emulsions in a microfluidic device, *Appl. Phys. Lett.* **88**, 024106 (2006).
- [8] P. Xu, X. Zheng, Y. Tao, and W. Du, Cross-interface emulsification for generating size-tunable droplets, *Anal. Chem.* **88**, 3171 (2016).
- [9] A. M. Gañán-Calvo, J. M. López-Herrera, M. A. Herrada, A. Ramos, and J. M. Montanero, Review on the physics electrospray: From electrokinetics to the operating conditions of single and coaxial Taylor cone-jets, and AC electrospray, *J. Aerosol Sci.* **125**, 32 (2018).
- [10] H. Kim, D. Luo, D. Link, D. A. Weitz, M. Marquez, and Z. Cheng, Controlled production of emulsion drops using an electric field in a flow-focusing microfluidic device, *Appl. Phys. Lett.* **91**, 133106 (2007).

- [11] H. Gu, F. Malloggi, S. A. Vanapalli, and F. Mugele, Electrowetting-enhanced microfluidic device for drop generation, *Appl. Phys. Lett.* **93**, 183507 (2008).
- [12] J.-C. Baret and F. Mugele, Electrical Discharge in Capillary Breakup: Controlling the Charge of a Droplet, *Phys. Rev. Lett.* **96**, 016106 (2006).
- [13] J. Eggers, Universal Pinching of 3D Axisymmetric Free-Surface Flow, *Phys. Rev. Lett.* **71**, 3458 (1993).
- [14] G. I. Taylor, Disintegration of water drops in an electric field, *Proc. R. Soc. London, Ser. A* **280**, 383 (1964).
- [15] N. Chetwani, S. Maheshwari, and H.-C. Chang, Universal Cone Angle of AC Electrosprays Due to Net Charge Entrainment, *Phys. Rev. Lett.* **101**, 204501 (2008).
- [16] Z. Pan, Y. Men, S. Senapati, and H.-C. Chang, Immersed ac electrospray (iACE) for monodispersed aqueous droplet generation, *Biomicrofluidics* **12**, 044113 (2018).
- [17] Z. Z. Chong, S. H. Tan, A. M. Gañán-Calvo, S. B. Tor, N. H. Loh, and N.-T. Nguyen, Active droplet generation in microfluidics, *Lab on a Chip* **16**, 35 (2016).
- [18] H.-C. Chang and L. Y. Yeo, *Electrokinetically Driven Microfluidics and Nanofluidics* (Cambridge University Press, New York, 2010).
- [19] H.-C. Chang, E. A. Demekhin, and E. Kalaidin, Iterated stretching of viscoelastic jets, *Phys. Fluids* **11**, 1717 (1999).
- [20] C. Xu, Z. Zhang, J. Fu, and Y. Huang, Study of pinch-off locations during drop-on-demand inkjet printing of viscoelastic alginate solutions, *Langmuir* **33**, 5037 (2017).
- [21] C. F. Eyring, S. S. Mackeown, and R. A. Millikan, Fields currents from points, *Phys. Rev.* **31**, 900 (1928).
- [22] A. R. Jones and K. C. Thong, The production of charged monodisperse fuel droplets by electrical dispersion, *J. Phys. D* **4**, 1159 (1971).
- [23] L. B. Loeb, A. F. Kip, G. G. Hudson, and W. H. Bennett, Pulses in negative point-to-plane corona, *Phys. Rev.* **60**, 714 (1941).
- [24] J. R. Lister and H. A. Stone, Capillary breakup of a viscous thread surrounded by another viscous fluid, *Phys. Fluids* **10**, 2758 (1998).
- [25] K. W. Ebagninin, A. Benchabane, and K. Bekkour, Rheological characterization of poly(ethylene oxide) solutions of different molecular weights, *J. Colloid Interface Sci.* **336**, 360 (2009).
- [26] L. C. Cerny and W. P. Walawender, The flow of a viscous liquid in a converging tube, *Bull. Math. Biophys.* **28**, 11 (1966).
- [27] R. Miller, P. Joos, and V. B. Fainerman, Dynamic surface and interfacial tensions of surfactant and polymer solutions, *Adv. Colloid Interface Sci.* **49**, 249 (1994).
- [28] V. Tirtaatmadja, G. H. McKinley, and J. J. Cooper-White, Drop formation and breakup of low viscosity elastic fluids: Effects of molecular weight and concentration, *Phys. Fluids* **18**, 043101 (2006).